Numerical Modeling of Thin Film Solar Cell with Hybrid 3D/2D Organic-Inorganic Halide Perovskite under Low Light Conditions and AM 1.5G Full Sun Spectrum.

N. L. Adihetty[a], D. R. Ratnasinghe[a], M.L.C. Attygalle[b*], Narayan N. Som[c], Prafulla K. Jha[c]

[a] Department of Graduate Studies, Faculty of Applied Sciences, University of Sri Jayewardenepura, Nugegoda, Sri Lanka
[b] Department of Physics, Faculty of Applied Sciences, University of Sri Jayewardenepura, Nugegoda, Sri Lanka
[c] Department of Physics, Faculty of Science, The M.S. University of Baroda, Vadodara 390002, India

* Corresponding author:

Email address: lattygalle@sci.sjp.ac.lk

Abstract

Organic-inorganic halide perovskite solar cells (PSCs) have received significant research attention due to their low processing cost and high performance. We have modeled perovskite thin-film solar cell, p-i-n structure, with intrinsic layers of bulk methylammonium lead iodide ($CH_3NH_3PbI_3$) and two-dimensional monolayer of $CH_3NH_3PbI_3$, which is mainly used to enhance the stability of bulk $CH_3NH_3PbI_3$ layer. Poly (3,4-ethylenedioxythiophene) polystyrene sulfonate (PEDOT: PSS), which is an organic hole transporting material (HTM), has been used as a p-type layer. The material fullerene derivative (6,6)-phenyl-C61-butyric acid methyl ester (PCBM), which is an organic electron transporting material (ETL), has been used as an n-type layer. The performance of this perovskite solar cell model was simulated by employing Solar Cell Capacitance Simulator (SCAPS-1D) under indoor low light conditions and outdoor AM1.5G full Sun spectrum. The indoor light intensity produced by the artificial light source is about 20 W/m² as compared to the outdoor light intensity of 1000 W/m^2. In this work, Tungsten Halogen lamps were used as low light illumination sources to model the indoor low light conditions. We have obtained the maximum power conversion efficiencies of the baseline model of PSCs under spectrums of 10 W, 20 W, 50 W Tungsten Halogen Lamps, and AM1.5G Sun as 11.47%, 12.04%, 12.16%, and 24.71% respectively with the open-circuit voltages (V_{OC}) of 1.07 V, 1.09 V, 1.12 V, and 1.26 V. According to these results, even for low light conditions, we have obtained open-circuit voltages above 1.0 V and the device efficiencies above 11% compared to outdoor light conditions.

Keywords: perovskite-based solar cell, power conversion efficiency, light intensity, SCAPS-1D, low light conditions

1. Introduction

Hybrid organic-inorganic halide perovskites have shown better performance because of their special properties, which are tunable optical bandgap, weak exciton binding energy, and suitable absorption coefficients(Chen et al., 2015). These properties are leading to high performance in photovoltaic. Perovskite solar cells (PSCs) are coming out as one of the clean energy production sources because they show low material cost, low processing cost, and overhead power conversion efficiencies (PCEs). The results of the national renewable energy laboratory (NREL) have proved that the power conversion efficiency of Perovskite solar cell has achieved as high as 25.2% in laboratories(Best Research-Cell Efficiency Chart). Optimizing layers, the progress of contact materials, improvement of interface studies, and new cell structures cause to acquire the high efficiency.

Organic-inorganic halide perovskites basically have general formula as ABX_3, A is a cation as CH_3NH_3+ (MA+), B indicates metallic cation (Pb^{2+}, Sn^{2+},..), and X interprets a halide ion (Cl^-, Br^-,....)(Mitzi, 2004). These kinds of mixed perovskite materials are called hybrid organic-inorganic halide perovskites. Among them, one of the widely studied 3D halide perovskites is methylammonium lead iodide (3D-$MAPbI_3$). Despite the $MAPbI_3$ shows good performance as a semiconductor material, this kind of materials are affected by some issues, which are lack of durability, and thermal instability(Krishna et al., 2019). Moisture instability, and exposing ultraviolet light cause to decrease the long-term performance of $MAPbX_3$, which can reduce the light-absorbing ability. Lattice structure conversion, halide segregation of $MAPbX_3$, and chemical decomposition lead to degradation of $MAPbX_3$(Barker et al., 2017). There are two methods to improve the durability in composition engineering, which are adding functional groups of hydrophobic organic molecules to perovskite material, and cation intermixing (including MA+ ion). The first method is used as an interface modification in composition engineering (Tang et al., 2017, Wang et al., 2018, Tiep et al., 2016, Yang et al., 2016). Improving the stability of $MAPbX_3$ is necessary to make a durable perovskite solar cell.

2D Ruddlesden-Popper halide perovskites can be utilized to overcome the stability issues of many 3D halide perovskite materials. Despite the optoelectronic properties of 2D perovskites have some limitations, two-dimensional perovskites have acquired the attention to solving the instability of three-dimensional perovskites. Optoelectronic limitations of 2D halide perovskites are narrow absorption range of the electromagnetic spectrum, short carrier diffusion length, and large exciton binding energy(Liu et al., 2018, Blancon et al., 2017). However, 2D halide perovskites have overcome the moisture instability because they have large hydrophobic organic cation, which can block the penetrating moisture (Quan et al., 2016, Cao et al., 2015, Koh et al., 2018). 2D layers of organic-inorganic hybrid perovskite have been manufactured (Dou et al., 2015), which cause to create new opportunities for photovoltaic research of halide perovskites. 2D halide perovskites have a general formula as $M_2(n)A_{n-1}B_nX_{3n+1}$, where M is a considerably large organic cation that can block the moisture(Gao et al., 2018). The n value of the general formula can be varied from 1 to infinity (∞). In the case of n=1, that material is considered as pure 2D single-layered perovskite. When n goes to infinity (∞), the 2D structure is going to be 3D structure. Other n values can make quasi 2D materials(Quan et al., 2016).

However, the combination of 2D and 3D halide perovskite layers has acquired more attention. In that combination, the 2D halide perovskite layer is doing an important role in which it acts as a protective layer to block the moisture and degrading of the 3D halide perovskite layer(Ma et al.,

2016, Grancini et al., 2017, Li et al., 2018a, Li et al., 2018b). This 3D/2D layer combination has shown higher moisture stability than a single 3D halide perovskite layer. The solar cell that has both 3D and 2D halide perovskite layers can be used to utilize the advantages of both 2D and 3D halide perovskites. The related density function theory (DFT) studies(Som et al., 2018, Kumavat et al., 2019) of 2D halide perovskites motivated to develop our numerical simulation of 3D/2D perovskite solar cell model. 2D perovskites show a narrow absorption band which also belongs to the ultraviolet and visible range of the electromagnetic spectrum. And also 2D perovskite show higher absorption coefficients which indicate that 2D perovskite can absorb more photons in the ultraviolet and visible spectrum. According to these points, a solar cell that is made with a 2D perovskite layer can work under low photon flux of the visible light. It may be helpful to make 3D/2D perovskite solar cells that can work under low light conditions. Due to this behavior of 2D perovskite, we can use 3D/2D perovskite solar cells for indoor applications because ultraviolet photons can be in the surrounding even a low light condition. By considering these properties of the 2D perovskite, we can use 3D/2D perovskite solar cell models as a solution for moisture stability and indoor applications. Nowadays, indoor photovoltaic applications have acquired popularity in the photovoltaic device market. Artificial light sources can be used to produce electricity with a solar cell that can generate electricity as an indoor application. Light sources that are normally used to light the surrounding emit the radiation which is in the visible range and non-visible range of the radiation spectrum. Lighting sources are wasting electrical energy, which can be partly utilized to generate electricity with a solar cell. Any devices that consume electrical power can harvest energy itself will be very useful to increase the alive time of the device.

2. Device structure and Effects of the different layers

The schematic device architecture of the cell model that is used is shown in Figure 1(a), and Figure 1(b) shows the energy level diagram of our solar cell model, which also illustrates the materials used to simulate this solar cell model. PEDOT: PSS is one of the conductive polymers, which has shown the highest efficiency among the conductive polymers. PEDOT: PSS is a standard chemical abbreviation of poly(3,4-ethylenedioxythiophene): poly(4-styrenesulfonate), which is hole acceptor material because the majority carriers of this layer are holes (Xu et al., 2019). This material is also considered as a transparent and flexible electrode to replace hard metallic oxides, as the Indium Tin Oxide (ITO). In this simulation study, PEDOT: PSS was selected as a p-type layer for this model because it is a hole transport material.

The performance of the solar cell can be enhanced by adding an absorber layer which can create both holes and electrons by absorbing photons. Methylammonium lead iodide (3D-MAPI) has 1.5 eV bandgap and shows relatively low exciton binding energy (below 26 meV)(Chen et al., 2018). Due to this low binding energy and high carrier diffusion length of 3D-MAPI, energy photons can easily separate electron and hole pairs. Here 3D-MAPI is selected as an intrinsic absorber layer, in which donor and acceptor density is equal to 10^{16} cm^{-3}. In the absorber layer, both electron and hole carrier mobility of 3D-MAPI is considered as 24 cm^{2}V^{-1}s^{-1}. Moving a hole from the main absorber (3D-MAPI) to the HTL layer (PEDOT: PSS) is not difficult because of the highest occupied molecular orbital (HOMO) value of PEDOT: PSS is higher than that of the absorber (3D-MAPI). In this solar cell model, two intrinsic absorber layers are used. One of them is 3D-MAPI and the other one is 2D-MAPI. Especially, the 2D-MAPbI$_3$ layer is used to improve

cell stability due to 2D Ruddlesden-Popper halide perovskite has shown good moisture stability, which will help to improve the solar cell stability(Ma et al., 2016). In this case, 2D-MAPI shows a direct bandgap as 1.63 eV, and it shows higher electron and hole mobility(Kumavat et al., 2019), 414 $cm^2V^{-1}s^{-1}$, and 1187 $cm^2V^{-1}s^{-1}$ respectively. These values of mobility indicate that the carrier mobility of this 2D-MAPI layer is higher than that of the 3D-MAPI layer. Normally, higher carrier mobility shows better device performance. 2D-MAPI has shown a narrow absorption band and strong absorption, which will cause to enhance the cell performance in the absorption band of 2D-MAPI (Boix et al., 2015, Som et al., 2018, Kumavat et al., 2019). And also 2D perovskites have shown higher exciton binding energy and low carrier diffusion length, which can cause to reduce the carrier separation in the layer and the overall cell performance.

PCBM is the abbreviation of the (6, 6)-phenyl-C_{61}-butyric acid methyl ester. This layer acts as an n-type layer because the majority carriers of this layer are electrons. In this solar cell modeling, PCBM is used as an electron acceptor material. The highest occupied molecular orbital (HOMO) and the lowest unoccupied molecular orbital (LUMO) of PCBM material are given -6.3 eV and -4.3 eV respectively, which shows its bandgap is 2.0 eV. According to these values, jumping electron from the absorber (2D-MAPI) to the ETL layer (PCBM) is not difficult due to the LUMO value of the PCBM layer is lower than that of the 2D-MAPI layer.

3. Methodology

3.1 Modelling Photovoltaic Device

In this study, we have prepared and characterized perovskite solar cell structure as a series of PEDOT: PSS/3D-perovskite/2D-perovskite/PCBM/Ag. The basic parameters used as initial inputs of this modeling were chosen from the literature (Olyaeefar et al., 2018, Som et al., 2018, Kumavat et al., 2019). We have simulated this perovskite solar cell model with different defects and different illumination sources. First, we have modeled the p-i-n type PSC baseline model without any point defects or interface defects. Next, the same PSC baseline model was simulated with only including point defects in 2D-MAPI. After that, the baseline model was simulated with only including point defects in 3D-MAPI. Also in the next case, point defects were included in both 3D-MAPI and 2D-MAPI. Finally, all these four cases were repeated with including interface layer defects between 3D-MAPI and 2D-MAPI.

The semiconductor parameters of the layers used for these simulations are given in Table 1. All the materials used to make this solar cell model are organic or hybrid organic-inorganic halide materials and consist of a large number of defects that have different types of defect distributions, which are shown in

Table 2. In this simulation study, amphoteric defect, which is one of the multivalent defects, are used for intrinsic materials because intrinsic materials may have donor type defects and acceptor type defects. Amphoteric defects contain three different charge states, which are 0, +1, and -1. Due to these reasons, amphoteric defects are selected as a defect type for intrinsic materials, with Gaussian defect distribution (Niemegeers et al., 2014, Meggiolaro et al., 2018). The effect of Shockley Read Hall recombination is considered through the different types of defects. The neutral interface defect layer is added to indicate the lattice mismatch of the 2D/3D lattice interface and decrease the carrier recombination at that interface. 3D-MAPI and 2D-MAPI indicate approximately equal lattice constants (a, b)(Kumavat et al., 2019), which might cause to decrease

defect density of 3D perovskite/2D perovskite interface. Adding a 2D/3D perovskite interface layer is important because 2D and 3D perovskite layers are intrinsic absorber layers that generate the carriers. That neutral interface layer indicates that there is considerably good contact between these two layers but there is a resistance to move the charge carriers. The influences of the series resistance and shunt resistance of the materials are not considered in this simulation study, and also the temperature of the solar cell model is set at 300 K.

3.2 Simulation

The J-V characteristics, open-circuit voltages, Fill Factors, and energy conversion efficiencies of PSCs were obtained under AM1.5G Sun incident light illumination (1000 W/m^2) using SCAPS-1D simulation software (Niemegeers et al., 2014). Also, we have modeled PSCs under different indoor illumination. We have used 10 W, 20 W, and 50 W power Tungsten Halogen lamps for different indoor low light conditions as illumination sources. We have included the illumination spectrums of Quartz Tungsten Halogen Lamps with different powers in the SCAPS-1D model to simulate the PSCs under the low light conditions. The incident power of illumination spectrums of Quartz Tungsten Halogen Lamps were extracted from the standard study (Data and Power). The spectral irradiance of the generic LED lamps and Tungsten Halogen lamps were compared and decided that the spectral irradiance of the Halogen lamp is higher than that of the LED lamp. But one small region of the LED spectrum showed higher spectral irradiance than the Halogen spectrum. However, by considering the whole spectrum, the Tungsten Halogen spectrum shows better performance than the LED spectrum as an illumination source in solar cell simulation.

4. Results and discussion

4.1 3D/2D halide Perovskite solar cell under low light condition

3D/2D perovskite materials are direct bandgap materials, with high absorption and narrow absorption band, which might be a better choice for the low-light conditions solar cells. Having a long carrier diffusion length in 3D perovskite materials causes to have high photocurrent in the solar cell, but 2D perovskite materials show low carrier diffusion length due to higher exciton binding energy. Perovskite solar cells generally show high open-circuit voltage (V$_{OC}$) under normal illumination condition (AM1.5G Sun), which indicate a low intrinsic loss. As a result, Perovskite solar cells are aspired to get good performance for indoor devices. The photon flux of incident photon is very low in low-light conditions and as a result, light-generated carrier transfer is less than the full solar spectrum illumination condition. Consequently, the short circuit current density (J$_{SC}$) values, under low-light conditions, are closer to dark current density values. J$_{SC}$, V$_{OC}$, and Fill factor should be increased to obtain higher efficiency under low-light conditions. Further, the interfacial recombination should be minimized to get high efficiency under low light conditions. The composition of absorber layers should be optimized for extremely low carrier concentration on working conditions. However, due to low carrier concentration and short carrier lifetime, the short circuit current density (J$_{SC}$) is low in low-light conditions.

In this simulation study, we have considered this model as a planar structure. Table 3 shows the photovoltaic performance parameters of the solar cell models under different illumination

conditions. Figure 2 and Figure 3 show current density vs voltage curves for different illumination sources, AM1.5G Sun spectrum and 50 W, 20 W, and 10 W Quartz Tungsten Halogen Lamps.

We have obtained the efficiency of the baseline model of PSC under spectrums of 10 W, 20 W, 50 W Tungsten Halogen Lamps, and AM1.5G Sun as 11.47%, 12.04%, 12.16%, and 24.71% respectively. The Australian National University has experimentally achieved halide perovskite solar cell with 21.6% efficiency under AM1.5G Sun spectrum(Green et al., 2019). We can compare our theoretical results with their experimental results. In our solar cell model, we have theoretically achieved 24.71% efficiency (Table 3) under AM1.5G Sun spectrum in the baseline model. Our theoretical results show an improvement in cell efficiency.

The efficiency losses can be explained due to the low carrier productions under low light conditions making an influential decay in the short circuit current densities. The short circuit current densities (J_{SC}) were reduced drastically when we use the low-light conditions (Quartz Tungsten Halogen Lamps). However, the open-circuit voltages (V_{OC}) were not reduced significantly under the low-light conditions. This behavior of 3D/2D halide perovskite solar cells explains the better performance under low light conditions. The efficiencies of 3D/2D halide perovskite solar cells are in the ranges, 11.47%-5.64%, 12.04%-6.05%, 12.16%-6.32% and 24.71%-14.09% for 10 W, 20 W, 50 W and AM1.5G Sun spectrum respectively, with different point and interface defects. According to Table 3, simulation results indicate that point defects of 2D-MAPI layer and 3D/2D interface defects mainly cause to reduce the cell efficiency, from the baseline model cell efficiency. The 2D-MAPI point defects and 3D/2D-MAPI interface defects should be controlled to get better performance in 3D/2D halide perovskite solar cells.

5. Conclusions

In summary, the efficiency of the 3D/2D perovskite solar cell was significantly reduced with the introduction of defects compared to the baseline model for both of the low light conditions and the AM1.5G Sun spectrum. Here, we have started with a baseline model without any defects and included 2D-MAPI point defects, 3D-MAPI point defects, and 2D/3D MAPI interface layer defects in the PSCs in different cases. Further, we investigated how the performance parameters such as Jsc, Voc, and FF of the PSCs vary under indoor illumination conditions and compared the results with outdoor illumination conditions. Indoor illumination conditions were tested using 10 W, 20 W, and 50 W spectrums of Quartz Tungsten Halogen Lamps. The efficiencies of 3D/2D PSCs are in the ranges, 11.47%-5.64%, 12.04%-6.05%, 12.16%-6.32% and 24.71%-14.09% for 10 W, 20 W, 50 W and AM1.5G Sun spectrum respectively. Irrespective to the illumination conditions, the open-circuit voltage (V_{OC}) values were consistent and in the range of 1.07 V to 1.26 V. Our findings revealed in this work will be useful to develop indoor applications of solar cells in the future.

Reference

BARKER, A. J., SADHANALA, A., DESCHLER, F., GANDINI, M., SENANAYAK, S. P., PEARCE, P. M., MOSCONI, E., PEARSON, A. J., WU, Y. & SRIMATH KANDADA, A. R. 2017. Defect-assisted photoinduced halide segregation in mixed-halide perovskite thin films. *ACS Energy Letters,* 2**,** 1416-1424.

BEST RESEARCH-CELL EFFICIENCY CHART. *Photovoltaic Research* [Online]. Available: https://www.nrel.gov/pv/cell-efficiency.html.

BLANCON, J.-C., TSAI, H., NIE, W., STOUMPOS, C. C., PEDESSEAU, L., KATAN, C., KEPENEKIAN, M., SOE, C. M. M., APPAVOO, K. & SFEIR, M. Y. 2017. Extremely efficient internal exciton dissociation through edge states in layered 2D perovskites. *Science,* 355**,** 1288-1292.

BOIX, P. P., AGARWALA, S., KOH, T. M., MATHEWS, N. & MHAISALKAR, S. G. 2015. Perovskite solar cells: beyond methylammonium lead iodide. *The journal of physical chemistry letters,* 6**,** 898-907.

CAO, D. H., STOUMPOS, C. C., FARHA, O. K., HUPP, J. T. & KANATZIDIS, M. G. 2015. 2D homologous perovskites as light-absorbing materials for solar cell applications. *Journal of the American Chemical Society,* 137**,** 7843-7850.

CHEN, Q., DE MARCO, N., YANG, Y. M., SONG, T.-B., CHEN, C.-C., ZHAO, H., HONG, Z., ZHOU, H. & YANG, Y. 2015. Under the spotlight: The organic–inorganic hybrid halide perovskite for optoelectronic applications. *Nano Today,* 10**,** 355-396.

CHEN, X., LU, H., YANG, Y. & BEARD, M. C. 2018. Excitonic effects in methylammonium lead halide perovskites. *The journal of physical chemistry letters,* 9**,** 2595-2603.

DATA, S. I. & POWER, C. O. ORIEL PRODUCT TRAINING.

DOU, L., WONG, A. B., YU, Y., LAI, M., KORNIENKO, N., EATON, S. W., FU, A., BISCHAK, C. G., MA, J. & DING, T. 2015. Atomically thin two-dimensional organic-inorganic hybrid perovskites. *Science,* 349**,** 1518-1521.

GAO, P., YUSOFF, A. R. B. M. & NAZEERUDDIN, M. K. 2018. Dimensionality engineering of hybrid halide perovskite light absorbers. *Nature communications,* 9**,** 1-14.

GRANCINI, G., ROLDÁN-CARMONA, C., ZIMMERMANN, I., MOSCONI, E., LEE, X., MARTINEAU, D., NARBEY, S., OSWALD, F., DE ANGELIS, F. & GRAETZEL, M. 2017. One-Year stable perovskite solar cells by 2D/3D interface engineering. *Nature communications,* 8**,** 1-8.

GREEN, M. A., DUNLOP, E. D., HOHL-EBINGER, J., YOSHITA, M., KOPIDAKIS, N. & HO-BAILLIE, A. W. 2019. Solar cell efficiency tables (Version 55). *Progress in Photovoltaics: Research and Applications,* 28.

KOH, T. M., SHANMUGAM, V., GUO, X., LIM, S. S., FILONIK, O., HERZIG, E. M., MÜLLER-BUSCHBAUM, P., SWAMY, V., CHIEN, S. T. & MHAISALKAR, S. G. 2018. Enhancing moisture tolerance in efficient hybrid 3D/2D perovskite photovoltaics. *Journal of Materials Chemistry A,* 6**,** 2122-2128.

KRISHNA, A., GOTTIS, S., NAZEERUDDIN, M. K. & SAUVAGE, F. 2019. Mixed dimensional 2D/3D hybrid perovskite absorbers: the future of perovskite solar cells? *Advanced Functional Materials,* 29**,** 1806482.

KUMAVAT, S. R., SONVANE, Y., SINGH, D. & GUPTA, S. K. 2019. Two-Dimensional CH3NH3PbI3 with High Efficiency and Superior Carrier Mobility: A Theoretical Study. *The Journal of Physical Chemistry C,* 123**,** 5231-5239.

LI, M. H., YEH, H. H., CHIANG, Y. H., JENG, U. S., SU, C. J., SHIU, H. W., HSU, Y. J., KOSUGI, N., OHIGASHI, T. & CHEN, Y. A. 2018a. Highly Efficient 2D/3D Hybrid Perovskite Solar Cells via Low-Pressure Vapor-Assisted Solution Process. *Advanced Materials,* 30**,** 1801401.

LI, P., ZHANG, Y., LIANG, C., XING, G., LIU, X., LI, F., LIU, X., HU, X., SHAO, G. & SONG, Y. 2018b. Phase Pure 2D Perovskite for High-Performance 2D–3D Heterostructured Perovskite Solar Cells. *Advanced materials,* 30**,** 1805323.

LIU, X., HUANG, T. J., ZHANG, L., TANG, B., ZHANG, N., SHI, D. & GONG, H. 2018. Highly Stable, New, Organic-Inorganic Perovskite (CH3NH3) 2PdBr4: Synthesis, Structure, and Physical Properties. *Chemistry–A European Journal,* 24**,** 4991-4998.

MA, C., LENG, C., JI, Y., WEI, X., SUN, K., TANG, L., YANG, J., LUO, W., LI, C. & DENG, Y. 2016. 2D/3D perovskite hybrids as moisture-tolerant and efficient light absorbers for solar cells. *Nanoscale,* 8**,** 18309-18314.

MEGGIOLARO, D., MOTTI, S. G., MOSCONI, E., BARKER, A. J., BALL, J., PERINI, C. A. R., DESCHLER, F., PETROZZA, A. & DE ANGELIS, F. 2018. Iodine chemistry determines the defect tolerance of lead-halide perovskites. *Energy & Environmental Science,* 11**,** 702-713.

MITZI, D. B. 2004. Solution-processed inorganic semiconductors. *Journal of Materials Chemistry,* 14**,** 2355-2365.

NIEMEGEERS, A., BURGELMAN, M., DECOCK, K., VERSCHRAEGEN, J. & DEGRAVE, S. 2014. SCAPS manual. *University of Gent.*

OLYAEEFAR, B., AHMADI-KANDJANI, S. & ASGARI, A. 2018. Classical modelling of grain size and boundary effects in polycrystalline perovskite solar cells. *Solar Energy Materials and Solar Cells,* 180**,** 76-82.

QUAN, L. N., YUAN, M., COMIN, R., VOZNYY, O., BEAUREGARD, E. M., HOOGLAND, S., BUIN, A., KIRMANI, A. R., ZHAO, K. & AMASSIAN, A. 2016. Ligand-stabilized reduced-dimensionality perovskites. *Journal of the American Chemical Society,* 138**,** 2649-2655.

SOM, N. N., SAMPATH, P., DABHI, S. D., MANKAD, V., SHINDE, S., ATTYGALLE, M. & JHA, P. K. 2018. Strain and layer modulated electronic and optical properties of low dimensional perovskite methylammonium lead iodide: Implications to solar cells. *Solar Energy,* 173**,** 1315-1322.

TANG, S., DENG, Y., ZHENG, X., BAI, Y., FANG, Y., DONG, Q., WEI, H. & HUANG, J. 2017. Composition engineering in doctor-blading of perovskite solar cells. *Advanced Energy Materials,* 7**,** 1700302.

TIEP, N. H., KU, Z. & FAN, H. J. 2016. Recent advances in improving the stability of perovskite solar cells. *Advanced Energy Materials,* 6**,** 1501420.

WANG, Q., LIN, F., CHUEH, C.-C., ZHAO, T., ESLAMIAN, M. & JEN, A. K.-Y. 2018. Enhancing efficiency of perovskite solar cells by reducing defects through imidazolium cation incorporation. *Materials today energy,* 7**,** 161-168.

XU, J., ZHU, Q., YILDIRIM, E., WANG, X., SOO, X. Y. D. S., ZHENG, Y., TAN, T. L., WU, G. & YANG, S.-W. 2019. Improved alignment of PEDOT: PSS induced by in-situ crystallization of "green" dimethylsulfone molecules to enhance the polymer thermoelectric performance. *Frontiers in Chemistry,* 7**,** 783.

YANG, S., WANG, Y., LIU, P., CHENG, Y.-B., ZHAO, H. J. & YANG, H. G. 2016. Functionalization of perovskite thin films with moisture-tolerant molecules. *Nature Energy,* 1**,** 1-7.
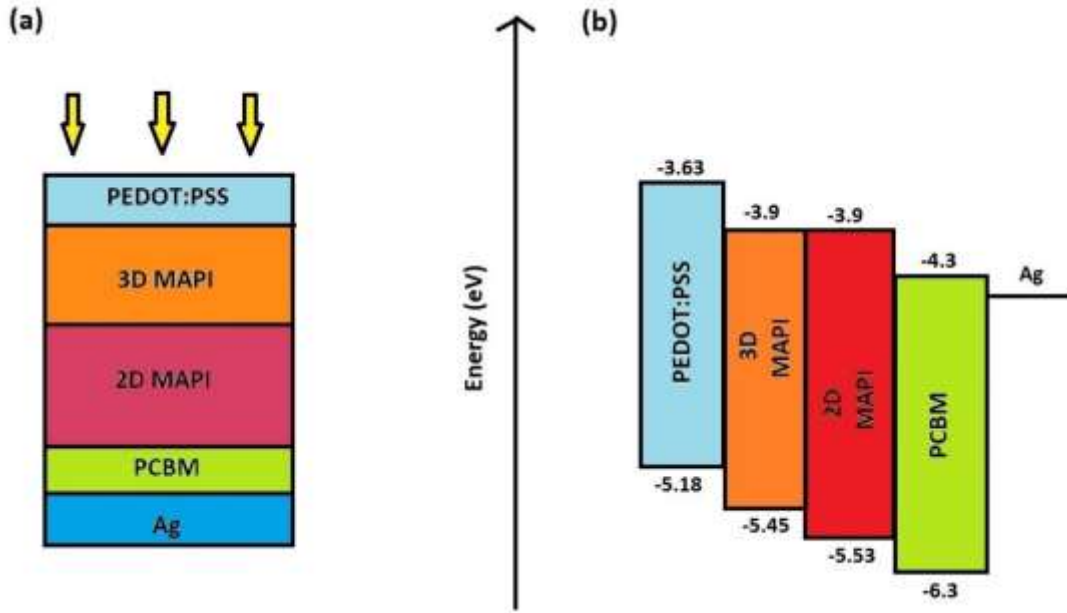
Figure 1: (a) Schematic device architecture and (b) a drawing of the energy levels through various layers of the device including PEDOT: PSS/3D perovskite/2D perovskite/PCBM/Ag.
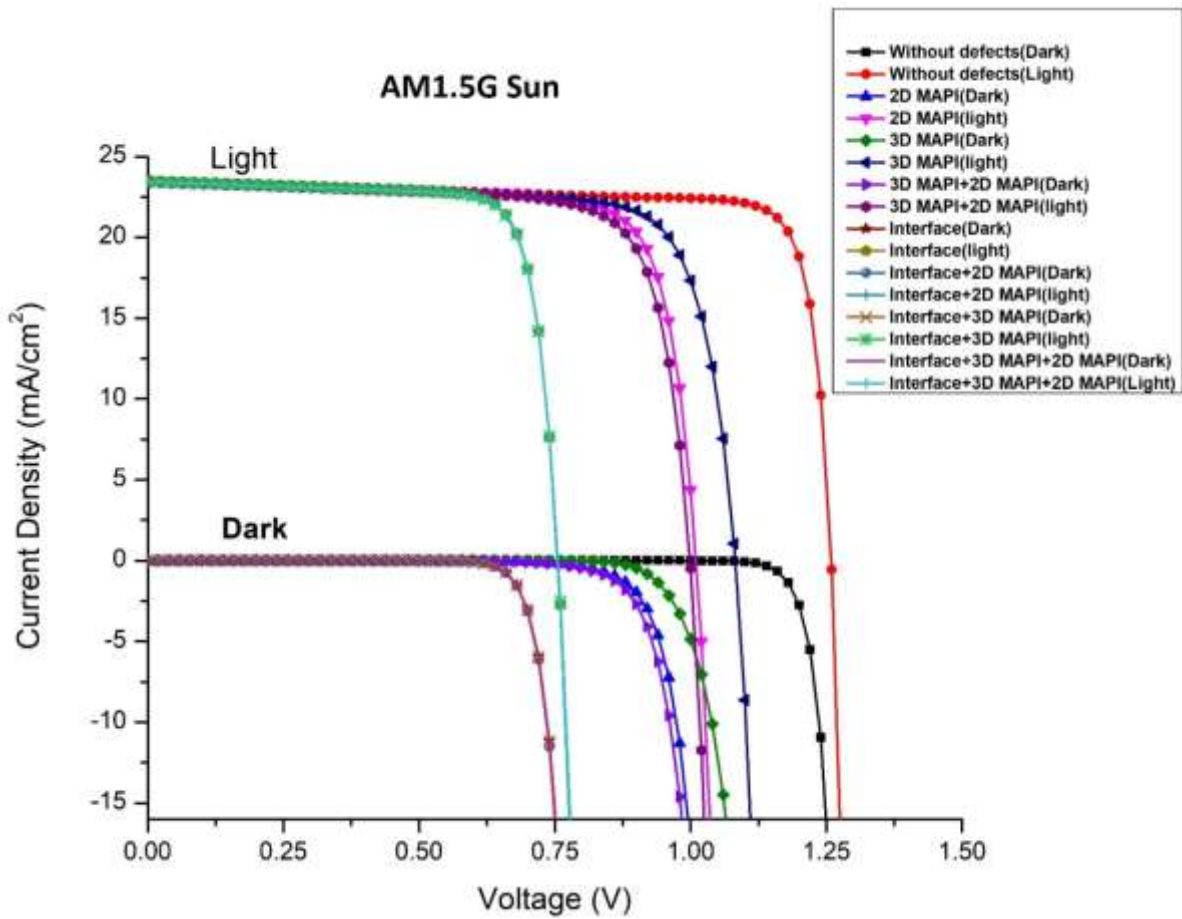

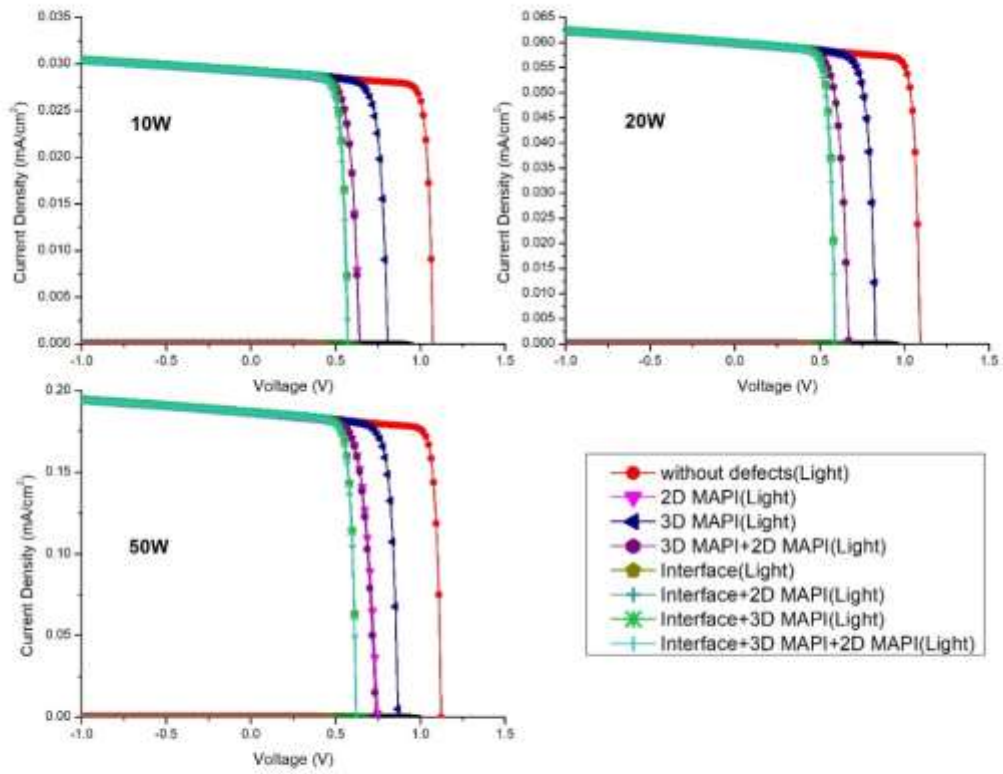*Figure 2: Current vs voltage curves for the AM1.5G Sun spectrum.*

Figure 3: Current vs voltage curves for 10W, 20W, and 50W tungsten bulb.

Table 1: The p-i-n perovskite Solar cell (baseline PSC) input parameters.

Material properties	PEDOT:PSS (HTL)	3D MAPI	2D MAPI	PCBM (ETL)
thickness (nm)	40	330	330	20
bandgap (eV)	1.55	1.5	1.63	2.0
electron affinity (eV)	3.63	3.9	3.9	4.3
dielectric permittivity (relative)	3	70	70	4
CB effective density of states ($1/cm^3$)	1E+19	2.8E+18	1.94E+20	E+19
VB effective density of states	1E+19	3.9E+18	1.94E+20	E+19
electron thermal velocity (cm/s)	1E+7	1E+7	1E+7	1E+7
hole thermal velocity (cm/s)	1E+7	1E+7	1E+7	1E+7
electron mobility (cm²/Vs)	9E-3	24	414	1E-2
hole mobility (cm²/Vs)	9E-3	24	1187	1E-2
shallow uniform acceptor density NA ($1/cm^3$)	3E+17	1E+16	1E+16	0
shallow uniform donor density ND ($1/cm^3$)	0	1E+16	1E+16	5E+17

Table 2: Defect parameters of interfaces and intrinsic layers.

Parameters	3D MAPI/2D MAPI interface	3D MAPI layer	2D MAPI layer
Defect type	Neutral	Amphoteric	Amphoteric
Capture cross section for electrons (cm^2)	1.00E-15	1.00E-15	1.00E-15
Capture cross section for electron (cm^2)	1.00E-15	1.00E-15	1.00E-15
Energy distribution	Gaussian	Gaussian	Gaussian
reference for defect energy level Et	Above middle of interface gap	Above EV	Above EV
energy with respect to Reference (eV)	0.6	0.6	0.6
characteristic energy (eV)	0.1	0.1	0.1
total density (integrated over all energies) ($1/cm^2$)	1.0E+15	1.0E+15	1.0E+15

Table 3: Photovoltaic parameters of solar cell models with different illumination conditions.

Illumination source	Added defect layers	PCE (%)	Voc (V)	Jsc (mA/cm^2)	FF (%)
AM1.5G Sun (1000W/m^2)	Without defects(baseline)	24.71	1.26	23.49	83.55
	2D MAPI (only)	18.53	1.01	23.46	78.18
	3D MAPI (only)	19.61	1.08	23.45	77.28
	2D MAPI,3D MAPI	17.97	1.00	23.43	76.81
	Interface	14.16	0.76	23.49	79.83
	Interface,2D MAPI	14.14	0.76	23.46	79.80
	Interface,3D MAPI	14.13	0.76	23.45	79.70
	Interface,3D MAPI,2D MAPI	14.09	0.76	23.43	79.59
10W Tungsten Bulb (2.32W/m^2)	Without defects(baseline)	11.47	1.07	29.29*10^{-3}	84.59
	2D MAPI (only)	6.05	0.64	29.25*10^{-3}	74.86
	3D MAPI (only)	8.02	0.81	29.78*10^{-3}	78.82
	2D MAPI,3D MAPI	6.06	0.64	29.24*10^{-3}	75.21
	Interface	5.79	0.57	29.28*10^{-3}	79.97
	Interface,2D MAPI	5.63	0.57	29.25*10^{-3}	78.58
	Interface,3D MAPI	5.79	0.57	29.27*10^{-3}	79.99
	Interface,3D MAPI,2D MAPI	5.64	0.57	29.24*10^{-3}	78.69
20W Tungsten Bulb (4.61W/m^2)	Without defects(baseline)	12.04	1.09	59.99*10^{-3}	84.66
	2D MAPI (only)	6.57	0.68	59.91*10^{-3}	74.79
	3D MAPI (only)	8.57	0.83	59.96*10^{-3}	79.35
	2D MAPI,3D MAPI	6.57	0.67	59.89*10^{-3}	75.24
	Interface	6.18	0.59	59.98*10^{-3}	80.26
	Interface,2D MAPI	6.05	0.59	59.91*10^{-3}	79.16
	Interface,3D MAPI	6.18	0.59	59.95*10^{-3}	80.28
	Interface,3D MAPI,2D MAPI	6.05	0.59	59.89*10^{-3}	79.25
50W Tungsten Bulb (14.62W/m^2)	Without defects(baseline)	12.16	1.12	186.97*10^{-3}	84.64
	2D MAPI (only)	6.98	0.75	186.73*10^{-3}	73.06
	3D MAPI (only)	8.87	0.87	186.86*10^{-3}	79.99
	2D MAPI,3D MAPI	6.96	0.74	186.63*10^{-3}	73.97
	Interface	6.41	0.62	186.95*10^{-3}	80.61
	Interface,2D MAPI	6.32	0.62	186.73*10^{-3}	79.88
	Interface,3D MAPI	6.41	0.62	186.84*10^{-3}	80.63
	Interface,3D MAPI,2D MAPI	6.32	0.62	186.63*10^{-3}	79.92